



Study of the Effect of *Artificial Gauge Field* on the Supersolid Phase in Cold Atomic Condensates

Research Article

Rashi Sachdeva, Sankalpa Ghosh*

Department of Physics, Indian Institute of Technology, New Delhi 110016, India

*Corresponding author: sankalpa@physics.iitd.ac.in

Abstract. Ultra cold atomic condensate with long range interaction is considered as a possible candidate to realize the supersolid phase. Such a supersolid phase can be subjected to artificial gauge field created either through rotation or by introducing space dependent coupling among hyperfine states of the atoms using Raman lasers. We study the effect of an artificial gauge field on the Supersolid phase in ultracold atomic condensates with long range interactions. Using Mean field approach, we demonstrate the structural differences between vortex in a supersolid and superfluid. We determine analytically the effect of the artificial gauge field on the density wave - supersolid (DW-SS) and the Mott insulator-superfluid (MI-SF) transition boundary. We also point out that in symmetric gauge the momentum distribution structure at these transition boundaries bears distinctive signatures of vortices in supersolid and superfluid phases. We point out that these results can clearly identify such a ultra cold atomic supersolid phase.

Keywords. Artificial gauge field ; Ultra cold atoms ; Supersolid

PACS. 03.75.Lm, 64.70.Tg, 67.80.bd

Received: May 15, 2013

Accepted: November 13, 2013

Copyright © 2014 Sankalpa Ghosh. *This is an open access article distributed under the Creative Commons Attribution License, which permits unrestricted use, distribution, and reproduction in any medium, provided the original work is properly cited.*

1. Introduction

Bose Einstein Condensate in gases with long range interactions are nowadays experimentally realizable in many systems. Some of the possible candidates are dipolar Cr^{52} gases [1], condensates with rydberg atoms [2] and with heteronuclear molecules [3]. These ultracold atomic systems provide new possibilities to explore quantum phases which arise due to the long range nature of interactions between the atoms. The effect of long-range interactions can

be minimally taken care of by considering the nearest neighbor interaction (NNI) in addition to onsite interactions to the Bose-Hubbard (BH) model [4]. Studying such condensates with long range interactions in deep optical lattices gives us a way to observe additional new phases such as Density wave (DW) and Supersolid (SS) phase in addition to Superfluid (SF) and Mott Insulator (MI) phases [5]. Of particular interest is the Supersolid phase, where the superfluid and crystalline orders co-exist i.e. this phase would achieve a coherent state that could allow matter to flow through the crystal. In recent experiments by Kim and Chan [6] on solid He^4 , there are signatures of the Supersolid phase in the system, but there are some debates on the interpretation of Supersolid phase in solid He^4 [7], so its existence is still questionable.

The Ultracold atomic systems loaded in an optical lattice can act as very promising candidates to confirm the existence of Supersolid phase and to explore the properties of this phase. In particular, the effect of artificial gauge field [8, 9] on the supersolid phase can give remarkable distinctive features as compared to superfluid phase and hence, the vortex structures in supersolid phases can act as signatures for detection of such phases. Within this general idea in mind, we have done the study of effect of artificial gauge field on the supersolid phase observed in the cold atomic quantum gases. We have studied the effect of gauge field on Supersolid phase [10] under a variational mean field approximation using Gutzwiller wave function by analytical means. In this work, the supersolid phase near the phase boundary, is shown to possess checkerboard vortex like structures which possesses density modulations in the superfluid order parameter. This study shows the structural differences in the vortex structures in supersolid and superfluid phase. It also shows the increase of the phase boundary of the insulating phases (DW and MI) as a function of increasing magnetic flux. The main results of this work and the formalism is given in Section 3.

In subsequent Section 4, we used the Strong Coupling Perturbation theory to calculate momentum distribution which is an experimentally relevant quantity, in presence of artificial gauge field. This technique is found to be quite accurate as it takes into account higher order corrections and dependence on the dimension of the system. We have analytically calculated the experimental signatures i.e. the momentum distribution of checkerboard vortex structures in Supersolid phase. This technique was able to produce more accurate phase diagram of the system in presence of gauge field, showing clearly the existence of various phases and the effect of gauge field on the transition boundaries of such phases. Most importantly, we were able to calculate the momentum distribution of the different phases, which is an experimentally relevant quantity and showed the distinct signatures of the vortex structures in a Supersolid as compared to vortex in a Superfluid.

2. Theoretical Framework

We consider cold atoms placed in a square optical lattice in two spatial dimensions, which is rotated in the plane about the z axis. The corresponding tight binding Hamiltonian in the corotating frame for cold atoms with on-site interaction and nearest neighbor interaction is

given by

$$H = - \sum_{i,j} t_{ij} \hat{b}_i^\dagger \hat{b}_j + \frac{1}{2} \sum_i \hat{n}_i (\hat{n}_i - 1) - \mu \sum_i \hat{n}_i + V \sum_{i,j} \hat{n}_i \hat{n}_j. \quad (1)$$

Here, the first term in above eq. (1) is the hopping term where the hopping matrix elements are non zero only for nearest neighbours and is given by $t_{ij} = t e^{i\phi_{ij}}$ with $\phi_{ij} = \int_{r_j}^{r_i} d\mathbf{r} \cdot \mathbf{A}(\mathbf{r})$ and $\mathbf{A}(\mathbf{r})$ is the vector potential corresponding to the artificial gauge field. Also, \hat{b}_i^\dagger , \hat{b}_i and \hat{n}_i are the boson creation, annihilation and number operators respectively. V is the strength of nearest neighbour interaction that captures the effect of nearest neighbor interaction, μ is the chemical potential. We have rescaled the Hamiltonian by U and thus, all parameters are measured in units of U . It is to note that we neglect the effect of an overall trap potential assuming that it is sufficiently shallow and is neutralized by the effect of centrifugal force particularly at the central region of the condensate.

For both the mean field and strong coupling calculations in the subsequent sections, we are interested in the limit $Vd < 1/2$, with d as the dimension. In this particular limit, the DW phase has the particle number distribution such that the adjacent lattice sites have n_0 and $n_0 - 1$ particles, and thus along the $t = 0$ axis, the system forms alternative sequence of $n_0 - \frac{1}{2}$ DW phases followed by n_0 MI phase.

It is very important to note that the actual physical interaction here is due to some sort of laser atom interaction which gives rise to an artificial gauge potential and not the artificial gauge field. And the system thus, does not show the true gauge invariance, and the fundamental quantities may not be necessarily gauge invariant. It can be seen from the momentum distribution results obtained in Section 4.2. This point has also been explained and emphasized in our work [11].

3. Mean Field Calculations

In this section, we use the variational mean field approach to carry out the minimization of the Hamiltonian (1) using the Gutzwiller wave function $|\Psi\rangle = \prod_i \sum_n f_n^i |n\rangle$. Here, f_n^i are the variational parameters which are amplitudes for the fock state $|n\rangle$ with N particles at site i . We determine the effect of artificial gauge field on the phase boundary of the DW phase and MI phase analytically by performing the energy minimization of eq. (1) using a reduced-basis variational ansatz for the Gutzwiller wave function near the phase boundary. For the DW phase, we can split the wave function as the product wave function for sublattice A and B , with n_0 and $n_0 - 1$ particles on each site, as $|\Psi\rangle = |\Psi_A\rangle |\Psi_B\rangle$. Here, $|\Psi_A\rangle = \prod_{i_A} \sum_{n_A} f_{n_A}^{i_A} |n_A\rangle$ and $|\Psi_B\rangle = \prod_{i_B} \sum_{n_B} f_{n_B}^{i_B} |n_B\rangle$, with $f_{n_A}^{i_A} = \delta_{n_A, n_0}$ and $f_{n_B}^{i_B} = \delta_{n_B, n_0 - 1}$. The minimization of the energy involves the expansion of the variational parameters in terms of the superfluid order parameters $\tilde{\phi}_A^{i_A}$ and $\tilde{\phi}_B^{i_B}$ of the two sublattices and neglecting the higher order corrections. The reader is advised to look at [10] for more explicit details of the calculation.

Minimization of the energy functional gives us the equations for the superfluid order

parameter, which can be written down as a spinorial Harper equation

$$\sum_{\langle i_A, i_B \rangle} (\hat{\mathbf{n}} \cdot \boldsymbol{\sigma}) \begin{bmatrix} \tilde{\phi}_A^{i_A} & \tilde{\phi}_B^{i_B} \end{bmatrix}^T = \frac{1}{\tilde{t}} \begin{bmatrix} \tilde{\phi}_A^{i_A} & \tilde{\phi}_B^{i_B} \end{bmatrix}^T. \quad (2)$$

Its solution can be written as $\tilde{\phi}(x, y) \otimes \left[\exp\left(-i\frac{\varphi_{i_A i_B}}{2}\right) \exp\left(i\frac{\varphi_{i_A i_B}}{2}\right) \right]^T$ where $\tilde{\phi}(x, y)$ satisfies the following symmetric gauge Harper equation (3)

$$\tilde{\phi}(x+1, y)e^{i\pi\nu y} + \tilde{\phi}(x-1, y)e^{-i\pi\nu y} + \tilde{\phi}(x, y+1)e^{-i\pi\nu x} + \tilde{\phi}(x, y-1)e^{i\pi\nu x} = \frac{1}{\tilde{t}} \tilde{\phi}(x, y). \quad (3)$$

$\frac{1}{\tilde{t}}$ in the right hand side of the eq. (3) can be mapped on the eigenvalues ε of Hofstadter butterfly spectrum plotted in Figure 1(a).

Here, we briefly mention the results obtained using the mean field formalism at the phase boundaries of the MI and DW phases. The edge of the Hofstadter butterfly spectrum (marked by black in color) gives the highest eigen value of the eq. (2) as a function of magnetic flux ν , which in turn is related to the minimum value of the hopping parameter t . This observation holds for the case of MI phase boundary too, by substituting $n_A = n_B = n_0$ in the calculations done for DW phase. It is found that the phase boundary of the DW and MI phase extends as a function of increasing strength of the gauge field. The reason behind this is the stronger localization of the bosonic states by the increasing strength of the artificial gauge field. It is shown in Figure 1(b), alongside the Hofstadter butterfly spectrum Figure 1(a).

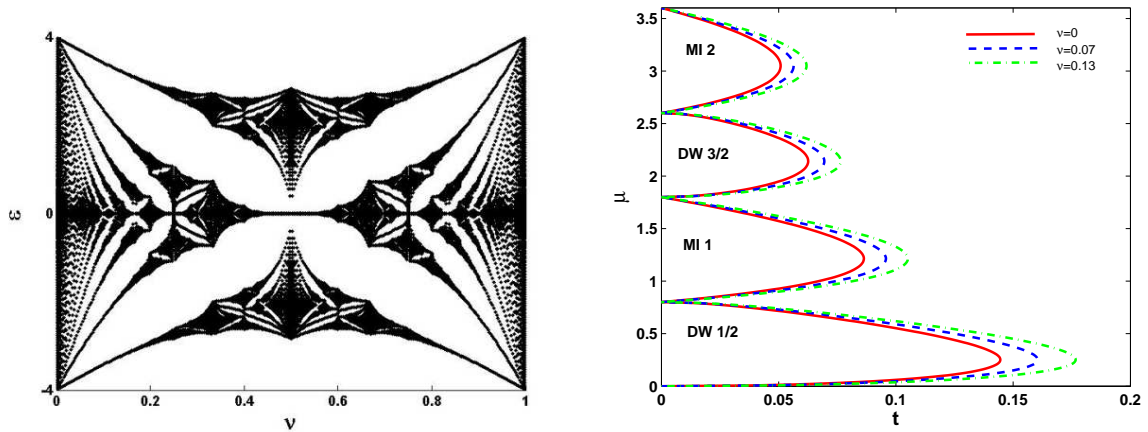


Figure 1. (a) Hofstadter butterfly spectrum, plotting the energy eigen values of Harper equation as a function of increasing magnetic flux. The highest eigen value marked black in color, gives the corresponding minimum values for the hopping parameter t . (b) Phase diagram of extended Bose Hubbard model under the effect of increasing magnetic flux, using mean field results.

Within our mean field analysis, we can also calculate the superfluid order parameter of the excitations at the boundary of both MI and DW phase. The order parameter near the DW phase for a given value of flux is found to be structurally very different from that of near the MI phase for same value of magnetic flux. This is because of the existence of supersolid phase near the DW phase in the phase diagram as compared to the SF phase near the MI

phase. It directly implies that the excitations in the supersolid phase are very different as compared to usual superfluid, and this is one of the main outcome of this mean field analysis. This has been demonstrated in Figure 2. This order parameter profile corresponds to the vortex structure in a supersolid phase and we can see that it indeed has structural differences than a vortex in a superfluid, shown in Figure 2 and hence, it can act as a signature for detection of supersolid phase in the system. Experimental techniques [12, 13] nowadays are able to detect such differences in sublattice modulated density and hence, can provide a robust signature for vortex in a supersolid.

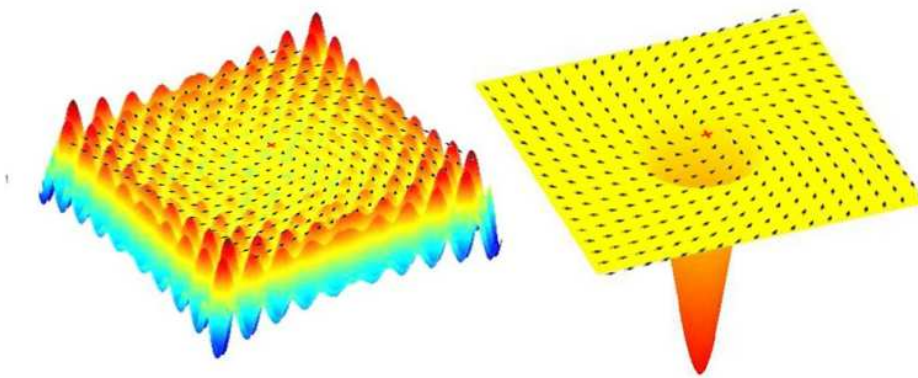


Figure 2. Structural difference between vortex in a supersolid and vortex in a superfluid.

4. Strong Coupling Perturbation Calculations

The strong-coupling perturbation expansion, used here to study the extended Bose Hubbard Model in presence of artificial gauge field, treats hopping parameter as a perturbation [14, 15], and it is found that the results from such an approach matches very well with results from quantum Monte Carlo simulations [16]. In this section, we describe the strong coupling perturbation formalism to determine the phase boundaries for the insulating phases (both DW and MI) and the momentum distribution of the phases at the boundaries in presence of an artificial gauge field. Within this formalism, we calculate the ground state energies and wave functions of the DW phase $E_{DW}(n_A, n_B)$ with n_A and n_B bosons on alternating lattice sites and MI phase $E_{MI}(n_0)$ with n_0 bosons on each lattice site, as a perturbative expansion in the hopping parameter t . We also calculate the energies of the DW and the MI states with an extra particle or hole, $E_{DW}^{par}(n_A, n_B)$, $E_{DW}^{hol}(n_A, n_B)$ and $E_{MI}^{par}(n_0)$, $E_{MI}^{hol}(n_0)$, using the perturbative expansion. It is to note that the energy of the DW and MI excitations (state with extra particle or hole) requires the use of degenerate perturbation theory, whereas the ground state of pure DW and MI state uses the non-degenerate perturbation theory. The unperturbed system corresponds to the case ($t = 0$).

4.1 Determination of phase boundaries of the insulating phases

The phase boundary between the DW phase and the SS phase is determined by

$$E_{DW}(n_A, n_B) = E_{DW}^{par/hol}(n_A, n_B). \quad (4)$$

Similarly, the phase boundary between the MI phase and the SF phase is determined as :

$$E_{MI}(n_0) = E_{MI}^{par/hol}(n_0). \quad (5)$$

Using the strong coupling perturbative expansion, one then obtains respective expressions for the energies of different insulating phases and the particle-hole excitations energies, and using eqs. (4) and (5), one then determines the chemical potential as a series expansion in powers of t . This gives us the corresponding μ values for different values of t and hence, one can trace the entire phase boundary of the insulating phases.

It is to note that in these calculations too, ϵ which is the minimum eigen value of the Hofstadter butterfly spectrum, enters in the series expansion and plays a major role in determining the effect of magnetic field on the phase boundary. The determination of the minimum eigenvalue ϵ involves the diagonalization of the hopping matrix, where the hopping matrix is dependent on the choice of the gauge potential. Thus, the location of the minimal eigenvalue ϵ depends on the choice of gauge potential, while the eigenvalue itself does not. For further details of the calculations, the reader is advised to look [11]. In above calculations, the DW state in the limit $Vd < 1/2$ can be obtained by putting $n_A = n_0$ and $n_B = n_0 - 1$ in above equations. The energies for the corresponding MI phase with n_0 particles at each lattice site can be obtained by carrying out a similar calculations. Please note that we are not providing here the complete calculations, and for details please refer to [11].

Figure 3 below shows the phase diagram of the extended bose hubbard model under the effect of increasing gauge field, using strong coupling expansion. This is obtained after doing a chemical potential extrapolation on the phase boundaries obtained by third order perturbative calculations [11]. This is because the accuracy of our calculations is restricted due to expansion up to finite order and hence, we use extrapolation technique to get more accurate results. Figure 3 also shows the increasing stability of the insulating phase (the DW and MI phases grow in size as the strength of the magnetic field is increased from zero to finite values), which is in agreement to the mean field results obtained [10]. The reason is again due to the localizing effect of magnetic field on the moving bosons, which favors the insulating phases to occupy a larger area in the phase diagram.

4.2 Momentum Distribution calculations

Experimental systems use the Time of flight absorption imaging of the freely expanding atoms to probe the properties of the cold atomic condensate with and without optical lattice. In such measurements, the quantity that is measured is the momentum distribution of the ultracold atomic systems. Here, we calculate the momentum distribution of such cold atomic condensates in presence of artificial gauge field within the framework of the strong-coupling expansion. We show that, in the presence of an artificial magnetic field, the momentum distribution actually

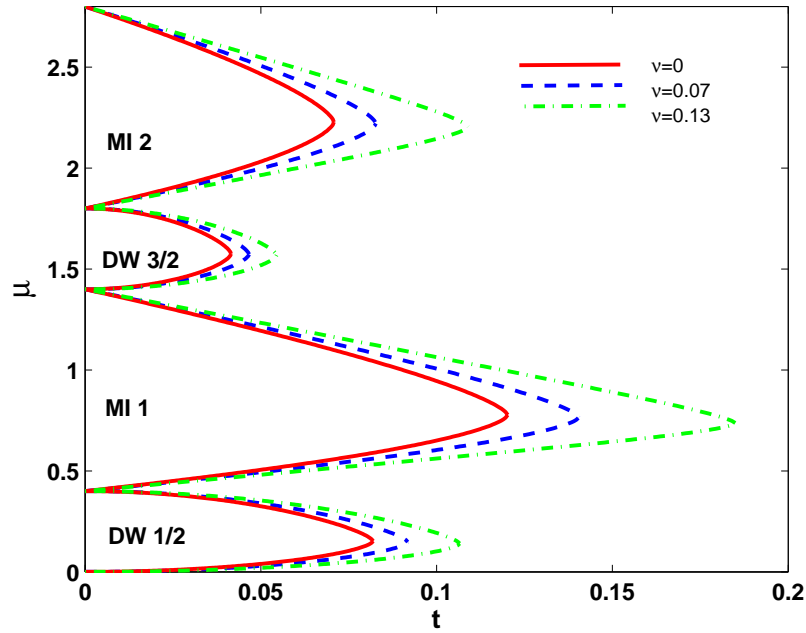


Figure 3. Phase diagram for the extended Bose Hubbard model, under the effect of increasing strength of magnetic flux with $Vd = 0.2$. The increasing area of the insulating lobes as a function of magnetic flux is due to the localizing effect of magnetic field on moving bosons.

depends on the means to produce such an effective magnetic field. The momentum distribution $n(k)$ is defined as

$$n(\mathbf{k}) = \int d\mathbf{r} \int d\mathbf{r}' \rho(\mathbf{r}, \mathbf{r}') e^{i\mathbf{k} \cdot (\mathbf{r} - \mathbf{r}')} . \quad (6)$$

It is the Fourier transform of the one-body density matrix $\rho(\mathbf{r}, \mathbf{r}') = \langle \psi^\dagger(\mathbf{r}) \psi(\mathbf{r}') \rangle$, with $\psi^\dagger(\mathbf{r})$ and $\psi(\mathbf{r})$ as the bosonic field operators. The strong coupling perturbation theory is used to calculate the corresponding wave function as a power series in the scaled hopping amplitude t . Using the wave function expansion of the DW and MI phases, we get the following expressions for the momentum distribution

$$\begin{aligned} n_{DW}(\mathbf{k}) = & \left(\frac{n_A + n_B}{2} \right) + \left[\frac{n_B(n_A + 1)}{E_1} + \frac{n_A(n_B + 1)}{E_2} \right] \epsilon(\mathbf{k}) \\ & + \left[\frac{n_B(n_A + 1)}{2E_1^2} + \frac{n_A(n_B + 1)}{2E_2^2} - \frac{n_B(n_A + 1)}{E_1} - \frac{n_A(n_B + 1)}{E_2} \right] \\ & \times (n_B + n_A + 1)(\epsilon^2(\mathbf{k}) - 2dt^2) + O(t^3), \end{aligned} \quad (7)$$

where

$$E_1 = (n_B - n_A - 1) + (zn_A - zn_B + 1)V,$$

$$E_2 = (n_A - n_B - 1) + (zn_B - zn_A + 1)V.$$

and

$$n_{Mott}(\mathbf{k}) = n_0 - \frac{2n_0(n_0 + 1)}{1 - V} \epsilon(\mathbf{k}) + n_0(n_0 + 1)(2n_0 + 1)(\epsilon^2(\mathbf{k}) - 2dt^2) \frac{3 - 2V}{(1 - V)^2} + O(t^3) \quad (8)$$

with the dispersion $\epsilon(k)$ as the minimum eigenvalue of the flux-dependent hopping matrix T or t_{ij} multiplied by a prefactor $2/M$ for the DW phase and $1/M$ for the MI phase, where M is the total number of lattice sites.

The artificial gauge field has distinctive effect on the MI-SF and DW-SS transition boundary and it is shown by plotting the momentum distribution derived in eqs. (7) and (8) in the k_x - k_y plane at these transition boundaries. It is because of the dependence of the matrix T on the gauge potential, that the momentum distribution reflects the gauge potential structure. Figure 4 below shows the momentum distribution profile for the DW and MI phase at the phase boundary for Landau gauge and symmetric gauge potential. One can see that the momentum distribution has an apparent gauge dependence on the specific type of the vector potential and not the field, in the typical experimental setups. This is one of the major observation of our work. Figure 4 also shows the distinctive features for a rotating supersolid near the DW phase boundary and a rotating superfluid near the MI phase, by appearance of extra peaks at the corners of reduced Brillouin zone at the DW phase boundary as compared to MI phase boundary. This is apparent for both choices of gauge potential i.e. Landau gauge and symmetric gauge potential. The small peaks happen to occur in the momentum distribution of DW even in the absence of a magnetic field, because of the presence of sub lattice structure of DW phase which results in reduced periodicity. On applying artificial gauge field, we observe small peaks in the DW momentum distribution at corners of the Brillouin zone, which is again attributed to the reduced periodicity of the DW phase compared to the MI phase. As mentioned before, momentum distribution can be measured using the Time of flight absorption imaging technique, this provides a way to experimentally distinguish between the supersolid phase and the superfluid phase by comparing the respective vortex profile.

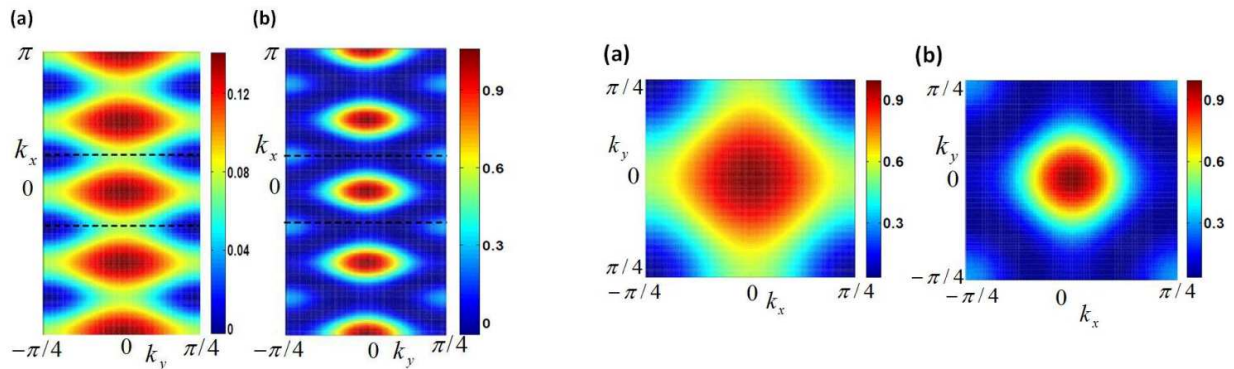


Figure 4. Momentum distribution at the phase boundary for MI phase, and DW phase in the reduced Brillouin zone corresponding to Landau gauge potential (left) and symmetric gauge potential (right).

5. Conclusion

To conclude, we have determined the modification of the DW-SS and MI-SF phase boundary for extended Bose Hubbard Model under the effect of an artificial gauge field using two approaches, mean field and strong coupling perturbation formalism. Within the mean field theory, we showed that the modification of phase boundaries of an EBH model due to an artificial

magnetic field can be derived from the highest eigen value edge spectrum of a spinorial Harper equation. We have also been able to calculate the vortex profiles for a supersolid phase and shown how it is structurally different from that of a superfluid. Further, using the strong coupling perturbation approach we have calculated the momentum distribution at the phase boundary of the insulating phases, which can be realized experimentally using TOF imaging. The momentum distribution is shown to reflect the symmetry of the gauge potential, and it also shows the distinctive features at the DW-SS phase boundary as compared with the MI-SF phase boundary. We hope that our calculation will stimulate further studies on the properties and behaviour of the SS phase under the effect of an artificial gauge field.

Acknowledgement

Rashi Sachdeva is supported by a fellowship given by CSIR, India and the work of Sankalpa Ghosh is supported by a grant from Planning section, IIT Delhi.

References

- [1] T. Lahaye *et al.*, Nature (London) **448**, 672 (2007).
- [2] N. Henkel, R. Nath and T. Pohl, Phys. Rev. Lett. **104**, 195302 (2010).
- [3] K.-K. Ni *et al.*, Science **322**, 231 (2008).
- [4] D. Jaksch *et al.*, Phys. Rev. Lett. **81**, 3108 (1998);
K. Sheshadri *et al.*, Europhys. Lett. **22**, 257 (1993).
- [5] D. L. Kovrizhin, G. V. Pai and S. Sinha, Europhys. Lett. **72**, 162 (2005).
- [6] E. Kim and M. H. W. Chan, Science **305**, 1941 (2004).
- [7] J. D. Reppy, Phys. Rev. Lett. **104** 255301 (2010);
N. Prokofév, Adv. Phys. **56**, 381 (2007);
P. W. Anderson, W. F. Brinkman and D. A. Huse, Science **310**, 1164 (2005).
- [8] K. W. Madison, F. Chevy, W. Wohlleben and J. Dalibard, Phys. Rev. Lett. **84**, 806 (2000);
S. Tung, V. Schweikhard and E. A. Cornell, Phys. Rev. Lett. **97**, 240402 (2006);
R. A. Williams, S. Al Assam and C. J. Foot, *ibid.* **104**, 050404 (2010).
- [9] Y.-J. Lin *et al.*, Nature **462**, 628 (2009).
- [10] R. Sachdeva, S. Johri and S. Ghosh, Phys. Rev. A **82**, 063617 (2010).
- [11] R. Sachdeva and S. Ghosh, Phys. Rev. A **85**, 013642 (2012).
- [12] M. Greiner *et al.*, Nature **415**, 39, (2002);
J. E. Simsarian *et al.*, Phys. Rev. Lett. **85**, 2040 (2000).
- [13] S. R. Muniz *et al.*, Phys. Rev. A **73**, 041605(R) (2006).
- [14] J. K. Freericks and H. Monien, Phys. Rev. B **53**, 2691 (1996).
- [15] J. K. Freericks and H. Monien, Europhys. Lett. **26**, 545 (1994).
- [16] W. Krauth, N. Trivedi and D. Ceperley, Phys. Rev. Lett. **67**, 2307 (1991).